Final Report

Dept. of Energy, Office of Fossil Energy

Federal Grant: DE-FE0031811

AOI 3 Life Modelling of Critical Steam Cycle Components in Coal-Fueled Power Plants

Awarded to Kratos SRE, Inc.

09/08/2023

PI: Dr Mark Patterson, Principal Scientist,
mark.patterson@kratosdefense.com (301) 221-8699(m)

This project was completed with generous support from our team member - Southern Company, Birmingham, AL

This report is not intended for public release until December 31, 2023.
Distribution authorized to U.S. Government agencies; To protect information not owned by the U.S. Government. This information is received with the understanding that it will not be routinely transmitted outside the U.S. Government.; Southern Company, Birmingham, AL

ACKNOWLEDGEMENT
This work was completed with support from the U.S. DOE, Office of Fossil Energy under the Federal Grant DE-FE0031811 and generous support from Southern Company.

1. EXECUTIVE SUMMARY

Microstructural damage accumulation models have been used to produce calibrated life estimation models for a DR22/P22 steel wye-block welds, and a Jethete stainless steel turbine blade (bucket). The calibrated life estimation models will aid the power plant operator in determining optimal maintenance and operation schedules based upon historical operational data as well as current, or future operation schemes. The impact of this project will enable existing coal-fueled power plants to operate safely for longer periods of time and at higher efficiencies, thereby reducing the economic and environmental impact of the existing coal power plant fleet.

Testing, characterization, and modelling indicates that the operating life of P22 pipelines and their welds are dominated by fatigue damage mechanisms. Specifically, fatigue is of no concern in these materials when operating under realistic conditions manifesting in the main steam piping of coal-fueled power plants. However, if a low-temperature overload ever occurs during operation, fatigue will manifest as a damage mechanism of interest. Primary impact provided by the completion of this work is in the manifestation of a detailed ABAQUS solid model providing accurate boundary conditions to enable the prediction of operational stresses and strains. The completed plant solid model, in conjunction with the calibrated fatigue and creep life models provide definitive confirmation that creep is the dominant damage mechanism during operational conditions.

Jethete life modelling has been completed by the manifestation of a material-specific, and temperature-specific, Kitagowa diagram. The Kitagowa diagram provides maintenance and operation decision making with scientifically-based go/no-go support based upon the crack-like features that have been identified by use of inspection.

2. GOALS AND PROGRAM OBJECTIVES

The goal of this research effort was to develop microstructurally based, calibrated life estimation models for a DR22/P22 steel wye-block welds, and a Jethete stainless steel turbine blade (bucket), and to show that these life models could provide insight into component operation and maintenance, thus benefitting the power generation industry. These two components were;

- Last stage (L-0) bucket turbine blade
  L-0 Last Stage Bucket (Turbine Blade) Water Droplet Erosion is a somewhat common, and very severe issue facing steam turbine operators.
  This work will answer “can failures be predicted from operational data and inspection findings”?
  This work will deliver calibrated life prediction and M&O scheduling models to enhance the performance and cost-effectiveness of coal-based power generation in the U.S. For the Jethete M-152 stainless steel the Failure Mechanism of Interest was identified as cracks emanating from these erosion pits.
- Wye block weld
  The main steam section of piping contains the wye block of interest that is exposed to thermal cycling during times as well as high internal pressures from the steam.
  The question being answered is “can we establish maintenance schedules to inspect the stability of welds exposed to this environment?
  This material is a DR22/P22 steel.

The calibrated life estimation models will aid the power plant operator in determining optimal maintenance and operations schedules based upon historical operational data as well as current, or

future operation schemes. The impact of this project is to enable existing coal-fueled power plants to operate safely for longer periods of time and at higher efficiencies, thereby reducing the economic and environmental impact of the existing coal power plant fleet.

3. RESULTS - JETHETE STAINLESS STEEL TURBINE BLADE (BUCKETS)

Last Stage Bucket leading edge erosion. Recent inspection of GE d11 unit with 20 years of service revealed severe erosion. Similar findings on coal unit last stage buckets with 30 years of service life were identified. The failures were linked to water droplet erosion – bucket tip liberation. Several failures occurred in the early 2000's on GE "self shielded" Jethete buckets. In 2005, GE released information indicating that self shielded rows 25-year failure rate was 1.4%. They also noted that cracks were initiated at erosion crevices near the bucket tip.

Figure 1. Images of the series of blades in question. The pitting of the trailing edges of the blades can clearly be seen in the higher resolution close-up images.

3.1 Background

The final stage buckets of steam-powered turbines often experience damage accumulation resulting from operational conditions coupled with water-droplet erosion. Ultimately, unfavorable operating conditions can lead to sufficient water droplet erosion so as to cause blade tip liberation. Water droplet erosion of several turbine blade materials in operational conditions has been studied for several decades[1],[2],[3],[4] [1-4]. It is generally understood that pitting caused by water droplet erosion may be modelled as a location of crack initiation. As the pit grows, the stress intensity (K in units of MPa-$m^{1/2}$) associated with the pit will become sufficiently large that the pit will behave like a sharp crack. At which point, a geometrically large crack resulting from the erosion pit may grow by steady, well defined rates, or the crack may grow uncontrollably and cause fast fracture. Crack initiation and growth as described above may be

[1] Salzman, R., Gandy, D., Rieger, N., Schönbauer, B., Tschegg, S., Zhou, S., Turnbull, A. *Corrosion-fatigue prediction methodology for 12% Cr steam turbine blades*. in *ASME Power Conference*. 2013. American Society of Mechanical Engineers.

[2] Salzman, R.N., Rieger, N.F., Tschegg, S., Schönbauer, B., Turnbull, A., Zhou, S., Gandy, D. *Corrosion-Fatigue in steam turbine blades*. in *Advances in Materials Technology for Fossil Power Plants: Proceedings from the Sixth International Conference*. 2011. ASM International Santa Fe, New Mexico.

[3] Macdonald, D.D., Engelhardt, G., *Predicting the future from the past in corrosion science and engineering.* 2004.

[4] *Nickel Based Superalloys*. [Web Page] 2003 [cited 2008 17 Apr]; Available from: <http://www.msm.cam.ac.uk/phase-trans/2003/Superalloys/superalloys.html>.

characterized by a materials fatigue crack growth (CFG) curve. A FCG curve is provided in Figure 2 for discussion.

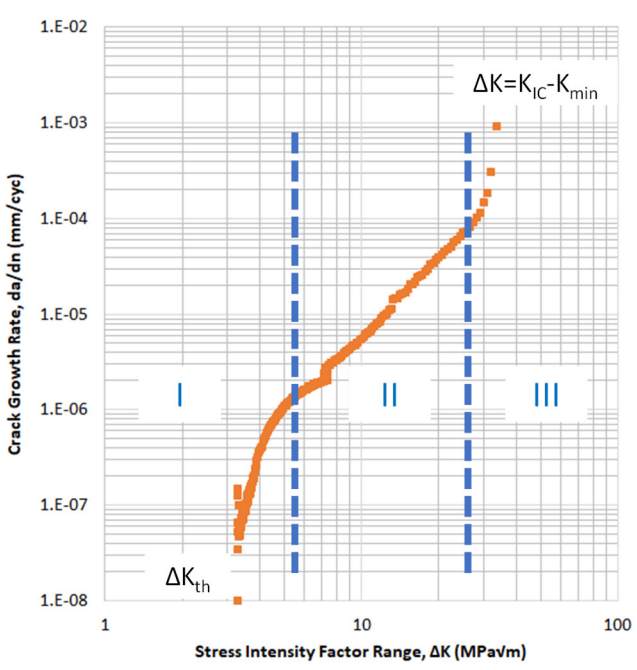

Figure 2: Fatigue crack growth data of Jethete M-152 at 93°C and a load ratio of R=0.56

Figure one depicts the results of a test in which a crack was grown in virgin Jethete M-152 at final stage bucket operational temperatures (93°C) and a load ratio of R=0.56. The load ratio is defined as

$$R = \frac{Load_{min}}{Load_{max}}, \qquad \text{EQ. 1}$$

where the $Load_{min}$ and $Load_{max}$ may have units of force, stress, strain, MPa-$m^{1/2}$, etc. The data is plotted as the fatigue crack growth rate (da/dN in mm of crack extension per cycle) versus the stress intensity factor range (ΔK in MPa-$m^{1/2}$). Fatigue crack growth data are typically separated into three regimes. Region I at the left is characterized by microstructurally small crack growth. Region I begins at the fatigue crack growth threshold (ΔK_{th}) value, below which a crack in existence will not extend. Note that the virgin Jethete M-152 data presented in Figure 1 exhibits a ΔK_{th} = 3.4 MPa-$m^{1/2}$. Region I microstructurally small crack growth transitions to Region II geometrically large, or the Paris FCG region crack growth at which point the FCG rate becomes constant. Fatigue crack growth in the Paris Region is characterized by steady, well defined fatigue crack growth rates defined by

$$\frac{da}{dN} = C\Delta K^m, \qquad \text{EQ. 2}$$

where C and m are material-, environment-, and loading-specific constants. When a crack has grown sufficiently large the FCGR will increase drastically as the crack quickly progresses to final fracture. Final fracture may be characterized by Charpy V-notch test values (CVN in N-m), fracture toughness values KIC in MPa-$m^{1/2}$), or it may be estimated by solving for the maximum stress intensity resulting in failure

during a FCG test. Note that the fracture toughness of the virgin Jethete M-152 tested at 93°C and R=0.56 is estimated to be K_{IC} = 60 MPa-m$^{1/2}$.

Closed-form solutions exist for stress intensity factors of crack existing in laboratory specimens as well as well-know geometries such as pits. The stress intensity range is defined generically by

$$\Delta K = \beta \cdot \Delta\sigma\sqrt{\pi a}, \qquad \text{EQ. 3}$$

where ΔK is the stress intensity range defined by $\Delta K = K_{max}$-K_{min}, β is a geometry specific factor, Δσ is the nominal stress range applied to the component/specimen of interest, and a is the crack length. Note that geometry factor is typically taken as β=0.65 for pits. If a component can be inspected, and a pit or a crack is located, one might determine if the crack will extend under operational conditions by comparing the stress intensity range experienced by the crack and the materials inherent FCG threshold. If the stress intensity range is larger than threshold value, one may then estimate the number of cycles that will be required for the crack to extend to some repair-critical length by differentiating Eq. 2. If, on the other hand an existing crack is not found during inspection, or if a component experiences unforeseen operational conditions after a crack has been located and deemed safe for operation, the crack may grow in an unstable manner, leading to fast fracture.

Separately, in many materials there exists an environmental-specific endurance strength, *Se*. If nominal component stresses are maintained below the material's inherent endurance limit (*Se*), the component would theoretically last indefinitely. The handbook values for endurance limit are typically tabulated for load ratios of R=-1. However, structures rarely experience fully reversed loading. In which case there are several relationships that can account for mean stress (i.e. R ≠ -1) effects in materials. The Gerber equation provided below

$$\frac{\sigma_{alt}}{UTS} = \frac{S_e}{UTS}\left[1 - \left(\frac{\sigma_{mean}}{\sigma_{alt}}\right)^2\right] \qquad \text{Eq. 4}$$

describes a relationship between the nominal alternating stress, σ_{alt}, the nominal mean stress, σ_{mean}, the materials ultimate tensile strength, UTS, and the materials endurance limit at R=-1, *Se* to account for mean stress effects in materials. Note that endurance limits are always determined as the stress that a component can withstand and not fail in a minimum of 10^6 cycles, and is often determined at a higher number cycles.

Combining the concepts of an endurance limit and a FCG threshold, Kitagowa[5] [5] determined that a failure assessment diagram of sorts could be created for materials and components having known loading conditions and known crack sizes. The Kitagowa Diagram for Jethete M-152 at 93°C and R=0.8 is provided in Figure 3.

[5] Kitagawa, H., *Applicability of fracture mechanics to very small cracks or the cracks in the early stage.* Proc. of 2nd ICM, Cleveland, 1976, 1976: p. 627-631

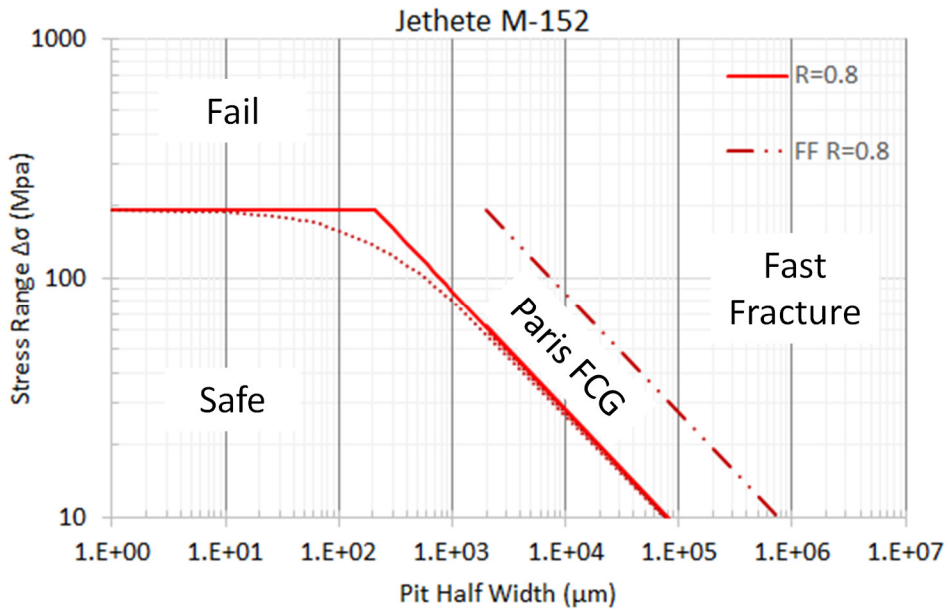

Figure 3: Amended Kitagowa Diagram for virgin Jethete M-152 at 93°C and R=0.8

The Kitagowa diagram in Figure 3 indicates a horizontal line at the materials endurance stress range ($\Delta\sigma_0=2\sigma_{alt}$) and a diagonal line at the materials FCG threshold value, both at a load ratio of R=0.8. The intersection of the two lines indicates the intrinsic crack or pit size for the environment and loading conditions. The intrinsic crack or pit size is defined as

$$c_0 \equiv \frac{1}{\pi}\left(\frac{\Delta K_{th}}{\beta \Delta\sigma_0}\right)^2 , \qquad \text{EQ. 5}$$

where all constants are defined above. Note that Figure 2 indicates that the intrinsic pit half width for virgin Jethete M-152 at 93°C and R=0.8 is C_0 = 211 µm. That is, under these environmental and loading conditions, a crack or pit having a measurable length under 422 µm would theoretically not extend at loads as high as $\Delta\sigma$ = 200 MPa. Above $\Delta\sigma$ = 200 MPa the component would not experience an infinite life. At lower stress ranges, crack having stress intensity factors larger than K_{th} will experience Region II or Paris Region FCG. If a crack extends sufficiently it will begin to grow uncontrollably and the component will experience fast fracture. This is indicated on Figure 3 by use of the dash-dot line. El Haddad and coworkers[6] [6] created a modification to the Kitagowa diagram that performs better at capturing experimental data while remaining conservative. The El Haddad line is described by

$$\Delta\sigma = \frac{\Delta K_{th}}{\beta\sqrt{\pi(c_0+c)}}, \qquad \text{Eq. 6}$$

Where all constants are defined above and is plotted as the dotted line in Figure 3.

Ultimately, the Jethete M-152 material characterization performed as part of this work is intended to support the power generation industry in optimizing inspection interval scheduling, as well

[6] El Haddad, M.H., Topper, T.H., Topper, T.N., *Fatigue life predictions of smooth and notched specimens based on fracture mechanics.* 1981.

as to provide a data-driven scheme to implement "retirement for a cause" methodology for final stage steam turbine blades. Failure of the final stage turbine blades experiencing water droplet erosion may result from any of the stages of damage accumulation experienced during service: crack initiation, microstructurally small crack growth to the point of critical crack existence, geometrically small crack growth to the point of steady state crack extension, long crack growth characterized by well-defined Paris regime, and/or fast fracture. Literature suggests that failiure under these loading and boundary conditions is characterized well by use of load-controlled high cycle fatigue testing to lives beyond 10^6 cycles, or a sufficient amount of cycles to capture the so-called endurance limit[1],[2] [1, 2]. This work will create multiple operational-specific Kitagowa diagrams for final stage turbine blades made of Jethete M-152 to incorporate endurance methods, crack initiation, and fast fracture in order to aid the power generation industry in both determining inspection methods of interests and scheduling inspection and overhaul operations based upon inspection data.

3.2 Material and Specimens

Virgin Jethete M-152 in forged bar form was sourced from Latrobe USA to support materials characterization for this work. A sufficient amount of material was sourced from a single heat/lot to create the following specimens:

- thirteen dogbones conforming to ASTM E8/E606 specifications in the longitudinal orientation,
- three sub-sized dogbones generally conforming to ASTM E8 in the transverse orientation,
- four compact tension specimens conforming to ASME E647 in the T-L orientation having W=2", and
- eight sub-sized compact tension specimens conforming to ASME E647/E399/E1820 in the T-L orientation having W=1".

Schematics of all specimen geometries tested as part of this program are provided in Figures 4 through 7. The virgin material's chemical composition, as provided in the Material Test Report/Certificate of Conformance, is provided in Table 1.

Table 1: Mill-provided Chemical Composition (measured) for the virgin Jethete M-152 Material

C	Mn	Si	P	S	Cr	Ni	Mo	V	N2	Cu	Fe
0.112	0.68	0.16	0.005	0.001	11.79	2.75	1.84	0.31	0.016	0.1	Bal

The Material Test Report indicates that the material exhibits an average ASTM grain size of 7, an ultimate tensile strength at room temperature of UTS = 1,085 MPa (175.4 ksi), a tensile yield strength at room temperature of σ_y = 947 MPa (137.4 ksi), an elongation to failure at room temperature of e_f = 21.3%, and a room temperature Charpy V-Notch impact value of CVN = 92 Ft-lbs.

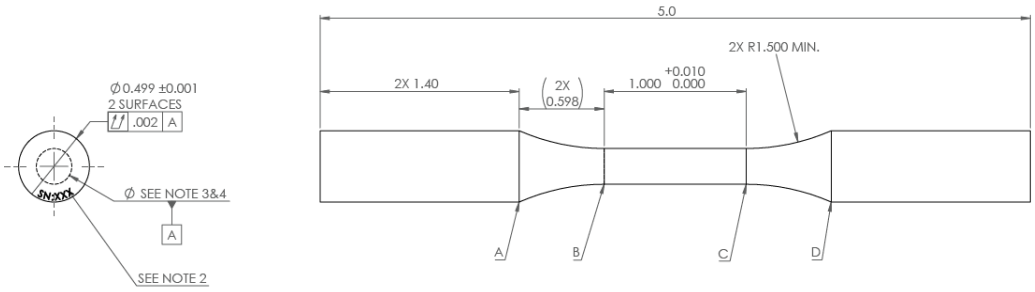

Figure 4: Tensile and fatigue specimen geometry used during this work. All specimens having longitudinal material orientations were created by use of this geometry. Geometry conforms to ASTM E8 and E606.

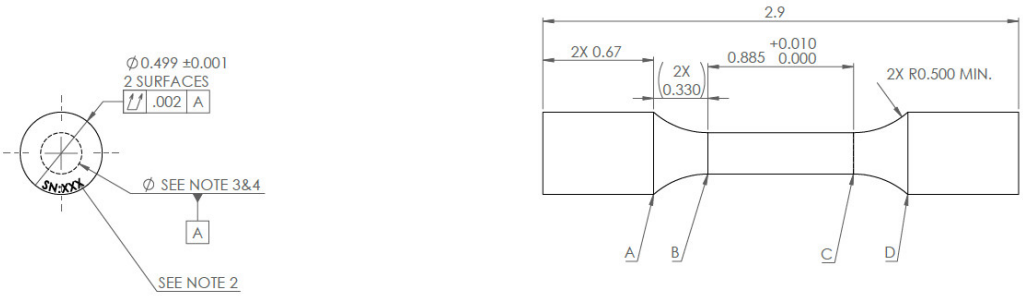

Figure 5: Sub-sized tensile specimen geometry used during this work. All specimens having transverse material orientations were created by use of this geometry. Geometry generally conforms to ASTM E8.

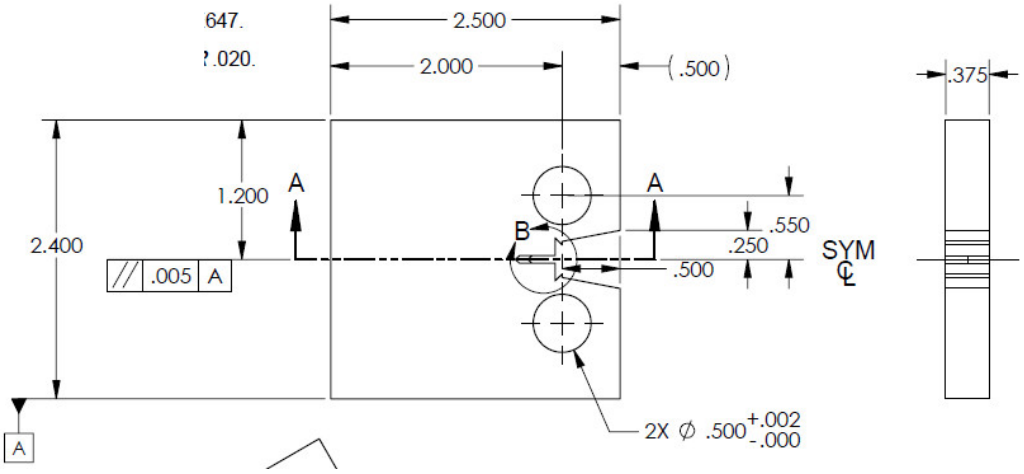

Figure 6: W=2” Contact Tension specimen geometry used during this work. All specimens have T-L orientations. Geometry confirms to ASTM E647.

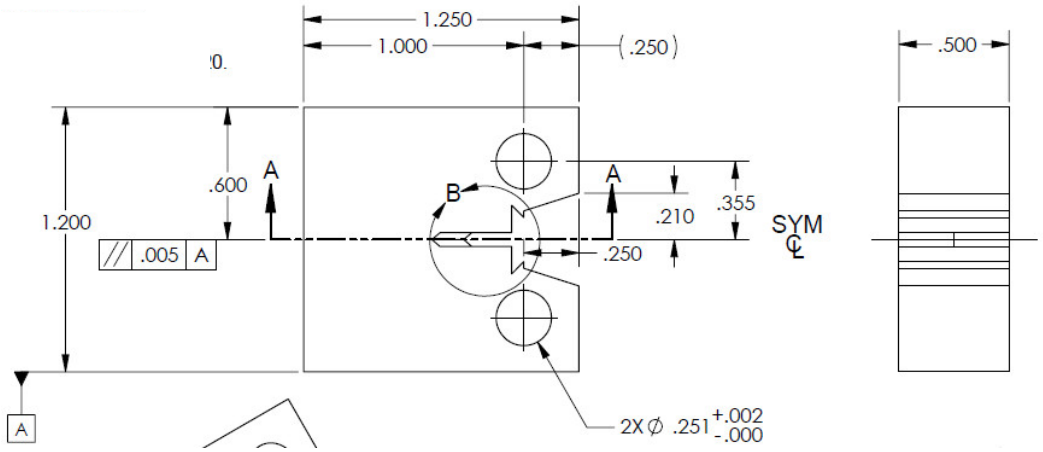

Figure 7: W=1" Contact Tension specimen geometry used during this work. All specimens have T-L orientations. Geometry confirms to ASTM E647, E399, and E1820.

3.3 Testing of Virgin Jethete M-152

Monotonic quasi-static tensile testing was performed on Jethete M-152 in the transverse direction at room temperature per ASTM E8. Additionally, a monotonic quasi-static tensile test was performed on the material in the longitudinal orientation at 90°C per ASTM E8. Tabulated test results are provided in Table 2. Engineering stress-strain data for each tensile test performed to date are provided graphically in Figure 8.

Table 2: Tabulated monotonic quasi-static engineering tensile results for Jethete M-152

Specimen	Material	Temperature	Orientation	E (Gpa)	Sig_Y (Mpa)	UTS (Mpa)	e_f (%)
01T	JH	25C	Transverse	210.0	836.7	1025.6	27.3
02T	JH	25C	Transverse	208.0	838.8	1027.8	27.1
D2L**	JH	90C	Longitudinal	185.0	804.9	978.0	**

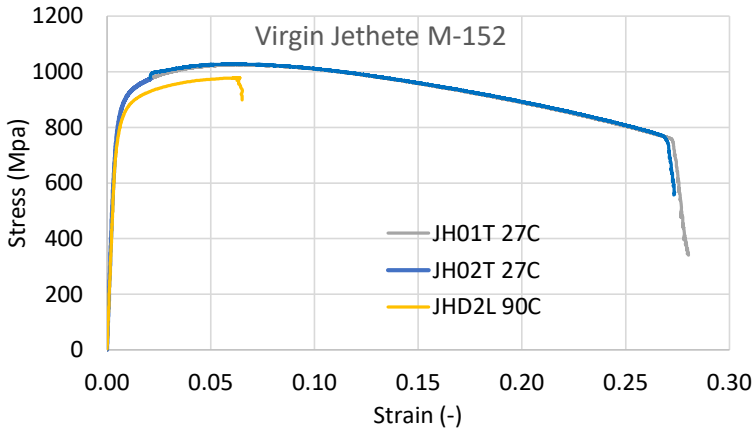

Figure 8: Quasi-static engineering stress-strain response of virgin Jethete M-152 at 27°C and 90°C.

Note that the elevated temperature tensile test experienced extensometer failure at the specimen's ultimate tensile strength. As such, strength values may be used from this test, but no conclusions can be drawn about the ductility of the material at this temperature. It is anticipated that three additional tensile tests will be performed as part of this work. The future tests will include one at room temperature in the longitudinal orientation, and two additional tests at 90°C in the longitudinal orientation.

Load-controlled high cycle fatigue (HCF) tests were conducted as part of this program to estimate the endurance limit of Jethete M-152 at 93°C and at various load ratios, R. Tabulated values of endurance testing performed as part of this work at 93°C and various load ratios is provided in Table 3.

Table 3: Test matrix/results for Jethete M-152, Stress-Life, 93°C, various load ratios. *Asterisk indicates test that were completed later. Values provided for incomplete tests are based upon literature and preliminary results.

Specimen	Temp	Mean	Alt	Min	Max	Max/UTS	$\Delta\sigma_0$	R	Nf
(#)	(deg C)	(Mpa)	(Mpa)	(Mpa)	(Mpa)	(%)	(Mpa)	(-)	(10^6 cycles)
JH01L	93	676.5	75.0	601.5	751.5	77%	150.0	0.80	>10
JHC2L	93	852.6	94.7	757.8	947.3	97%	189.5	0.80	>2.5
*N/A**	*93*	*734.2*	*213.1*	*521.0*	*947.3*	*97%*	*426.3*	*0.55*	*N/A*
*N/A**	*93*	*455.9*	*412.5*	*43.4*	*868.4*	*89%*	*824.9*	*0.05*	*N/A*

The test data provided in Table 3 (specimens JH01L and JHC2L) has been augmented by estimated endurance tests results (indicated by *) which have been projected by use of the initial test data and literature values.

Literature data suggests that the fully reversed endurance limit (Se) for Jethete M-152 at 93°C could range between Se = 380 MPa (55 Ksi) and Se = 585 MPa (85 ksi), depending upon the material Class[7] [7]. As such, it is expected that the virgin Jethete material tested here has a fully reversed fatigue limit/endurance limit of approximately Se = 550 MPa (80 ksi) at 93°C. Using this information, in conjunction with the experimentally determined ultimate tensile strength of UTS = 978 MPa at 93°C, one can estimate the mean stress effects exhibited by Jethete during endurance limit (or presumed infinite life) operating conditions. Prior work has shown that the Gerber Equation (EQ. 4 above) predicts the mean stress effects in 12% Cr stainless steels well[1],[2] [1, 2]. The Gerber Equation for Jethete M-152, solved for Se/UTS = 550 MPa/978 MPa = 0.56, is plotted in Figure 8. Note that Prior work[2] [2] solved for Se/UTS = 0.58 by fitting the Gerber Equation through experimental endurance limit data. Figure 9 includes the results of the R=0.8 endurance tests performed as part of this work (closed circle and star), as well as the predicted results of R=0.55 and R-0.05 endurance results yet to be completed (open circles). Note that endurance testing of Jethete at 93°C and load ratios of R-0.55 and R=0.5 are currently underway.

[7] Boyer, H., E., *Atlas of fatigue curves*. 1985: ASM International.

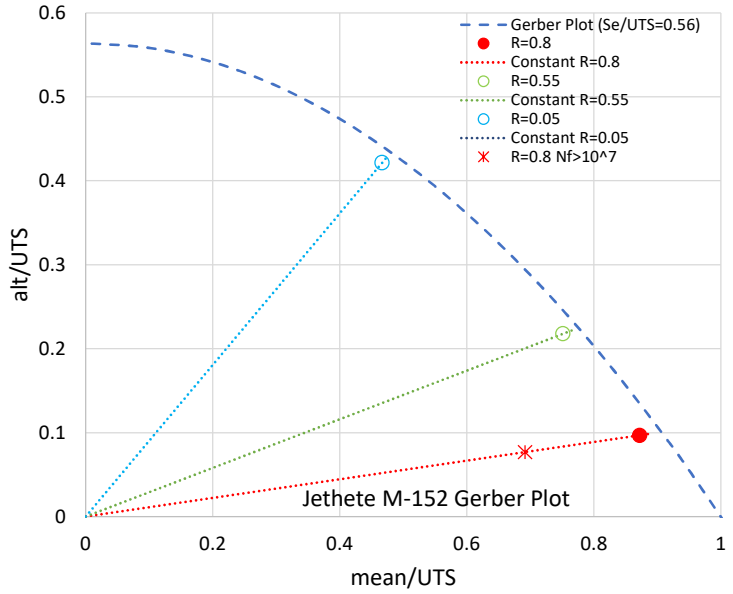

Figure 9: Gerber Plot of preliminary endurance limit fatigue data for Jethete M-152 at 93°C. *Open Circles indicates tests completed later in study. Values provided are estimates based upon literature and preliminary results.

The preliminary data presented in Figure 9 is promising in that the data collected to date coincides with Gerber model predictions, and is in-family with data collected by the Electric Power Research Institute and others[2] [2] on similar materials.

Fatigue crack growth (FCG) and FCG threshold (ΔK_{th}) testing was performed on the virgin Jethete M-152 at 93°C and at various load ratios. Tabulated FCG threshold results are provided in Table 4.

Table 4: Fatigue crack growth threshold test results for Jethete M-152 at 93°C.

Specimn	Temp	Test	ΔK_{th}	R
(#)	(deg C)	Control	MPa-√m	(-)
FTO-5	93	constant K_{max}	3.4	0.56
FTO-6	93	constant K_{max}	3.5	0.54
FTO-7	93	K decreasing	4.7	0.05
FTO-8	93	K decreasing	3.2	0.8

The FCG data provided in Table 4 is in-family with materials of similar chemical and microstructural composition[1] [1]. The calibrated Paris Equation constants (Eq. 2) for all FCG data collected as part of this work are tabulated in Table 5.

Table 5: Paris Values of fatigue crack growth test results for Jethete M-152 at 27°C, 93°C, and various load ratios.

Specimn	Temp	Test	R	C	m
(#)	(deg C)	Control	(-)		
FTO-5	93	Load- increasing ΔK	0.56	1.11×10^{-8}	2.73
FTO-6	93	Load- increasing ΔK	0.54	1.21×10^{-8}	2.73
FTO-7	93	Load- increasing ΔK	0.05	8.89×10^{-9}	2.62
FTO-8	93	Load- increasing ΔK	0.8	N/A	N/A
FTO-1	27	Load- increasing ΔK	0.1	1.44×10^{-8}	2.84
FTO-2	27	Load- increasing ΔK	0.1	1.15×10^{-8}	2.94

All of the FCG test data collected as part of this work are provided in Figure 9.

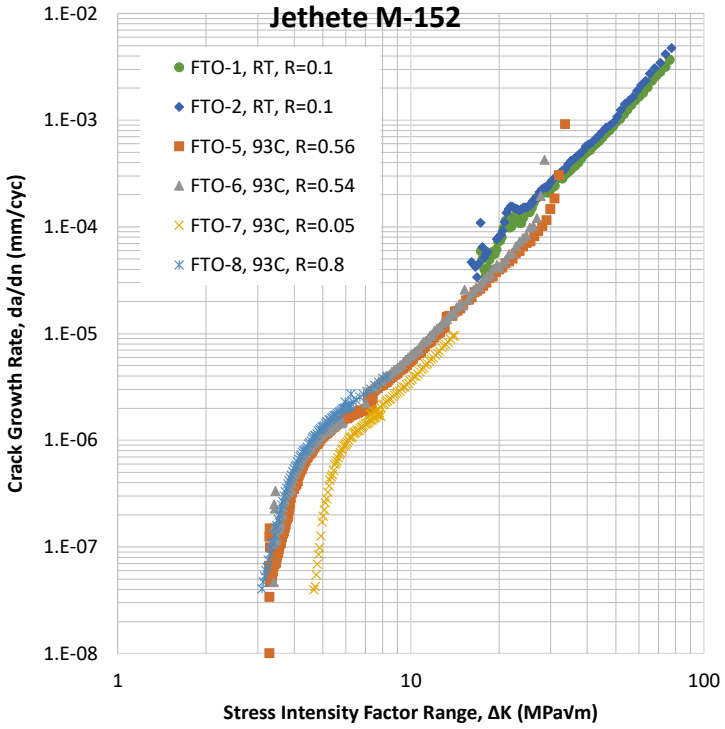

Figure 10: Fatigue Crack growth test results of Jethete M-152 at various temperatures and load ratios.

The data tabulated in Tables 4 and 5 and shown graphically in Figure 10 indicates that while the material may exhibit load ratio dependent FCG threshold values, the steady state long crack FCG regime (described by the Paris Equation) is (relatively) insensitive to load ratio, for the load ratios tested. Furthermore, the limited data collected suggests that the materials FCG response is insensitive to temperature changes between room temperature and 93°C. Figure 11 shows the crack threshold values and inherent critical crack size for the virgin Jethete M-152 at 93°C versus load ratio.

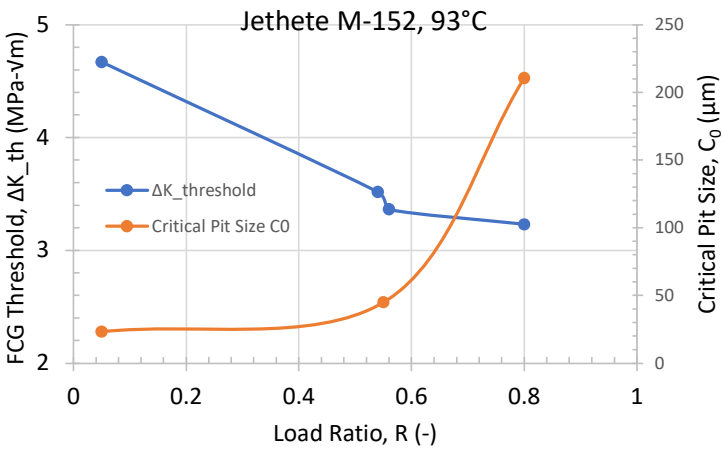

Figure 11: Fatigue crack growth threshold values for virgin Jethete M-152 at 93°C versus load ratio, and inherent critical crack size values for virgin Jethete M-152 at 93°C versus load ratio.

3.4 Finite Element Modeling of the L0 Buckets made from Jethete M152.

The FE model incorporates realistic boundary conditions to include interactions with the rotor/disk, the mid-span vibrational dampening connection, and the blade tip constraint. Loading conditions consist of centripetal accelerations resulting from operational turbine conditions in addition to the operating fluid pressure drop across the turbine. The FE results are provided in Figure 12.

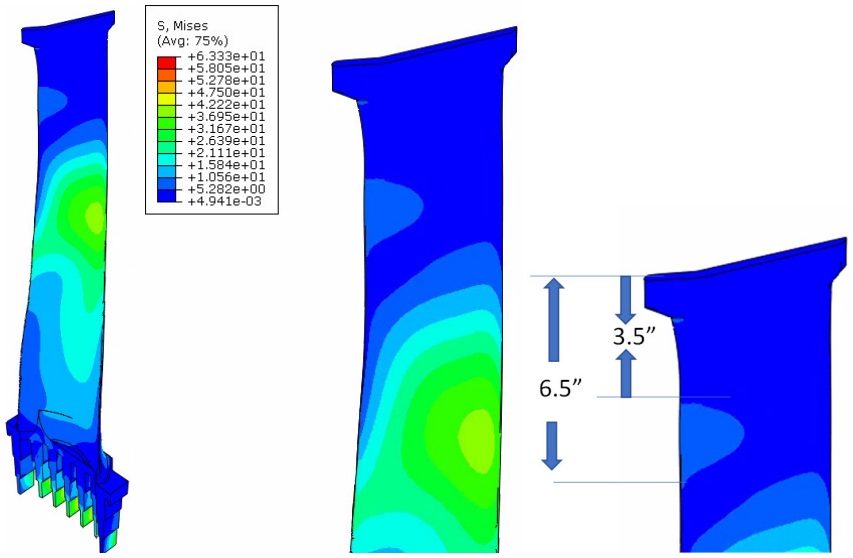

Figure 12: von Mises stress results estimate from finite element analysis. Note the local stress “hot-spot” located approximately 3.5” below the tip. This location roughly corresponds to that producing the highest erosion kinetics found from 18+ years of inspection data.

The data presented in Figure 12 indicates that the blade will experience mean stresses on the order of 45 ksi during operational conditions. Additionally, the data indicates that there is a local stress hot-spot roughly corresponding to the location of maximum erosion kinetics found during the erosion inspection data review. The results of the analysis of 18 years of inspection data collected from four separate turbines is provided in Figure 13.

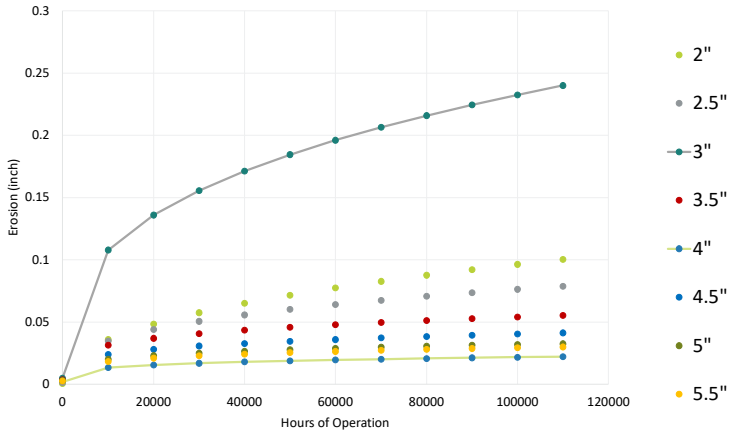

Figure 13: Collection of erosion inspection data from 4 turbines over 18 years. A location 3" down from the tip of the L0 bucket exhibits greatest water droplet erosion rates.

Elevated temperature endurance testing of Jethete M152 continued during Q7. Three HCF tests were performed at a load ratio of R=0.55. Results indicate that the material exhibits a lower Se/UTS ratio than that found for a similar material used for L0 buckets[8] [1]. Endurance testing will continue to finalize the calibration of the Kitagowa Diagram currently show in Figure 14.

[8] Salzman, Ronald, David Gandy, Neville Rieger, Bernd Schönbauer, Stefanie Tschegg, Shengqi Zhou, and Alan Turnbull. "Corrosion-fatigue prediction methodology for 12% Cr steam turbine blades." In *ASME Power Conference*, vol. 56055, p. V001T04A002. American Society of Mechanical Engineers, 2013

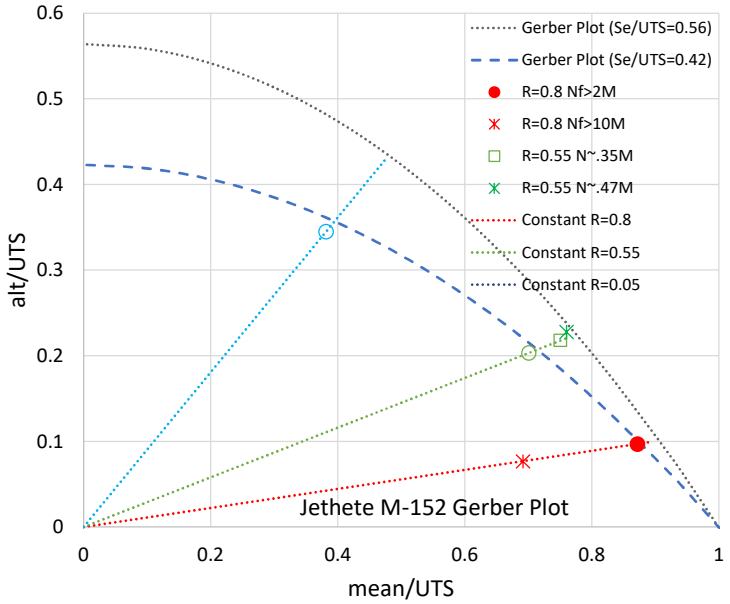

Figure 14: Updated Kitagowa Diagram for Virgin Jethete M152

3.5 Inspection Interval Scheduling and Failure Modelling

The failure and crack initiation testing performed as part of this work (endurance limit and FCG threshold) has been combined into a preliminary Kitagowa Diagram to elucidate safe operational conditions for this material at operational temperature (93°C). Specifically, when a component alternating stress, or stress range is known for a given loading ratio, one can use an appropriate Kitagowa Diagram to determine safe operating conditions relative to pits and cracks that may be in existence. The preliminary Kitagow Diagrams are provided in Figure 15 and the data collected to date to create the Kitagowa Diagram is tabulated in Table 6.

Table 6: Preliminary test values for Jethete M-152 at 93°C used in creating the preliminary Kitagowa Diagram. Asterisk indicates test that are yet to be completed. Projected values provided based upon literature and preliminary results.

R	$\Delta\sigma_0$	ΔK_{th}
(-)	(Mpa)	MPa-√m
0.05	824.9*	4.7
0.55	426.3*	3.4
0.80	189.5	3.2

Figure 15: Preliminary Kitagawa Diagrams (solid and dashed lines) plotted with El Haddad modification (dotted lines) for Jethete M-152 at 93°C. *Dashed stress range lines indicate tests that have yet to be completed. Projected values are based upon prior work and literature data.

One will note that a Kitagowa Diagram predicts "safe" operating conditions when the loading conditions (alternating stress or stress range) and boundary conditions (crack or pit half width) in existence may be plotted within the bottom-left portion of the Kitagowa Diagram. Within the bottom left portion of the diagram, microstructurally small crack growth is believed to occur. Above and to the right of the lines plotted on the Kitagowa diagram indicates either geometrically large crack growth or fast fracture. In its simplest use, the Kitagowa Diagram may be used as a go/no-go diagram. In general, for alternating loads below 200 MPa, and pits having widths less than approximately 400 µm (200 µm half width), the Kitagowa Diagram provided in Figure 15 predicts that a component is operating in a "safe" zone. Typical operating conditions for the L0 (final stage) bucket often result in alternating stress ranges on the order of 30 MPa-60 MPa at load ratios of 0.8 or greater[1][1]. The preliminary Kitagowa Diagram detailed in Figure 10 indicates that, at an operational stress range of 60 MPa and R=0.8, pits or crack under 1mm in half width will not extend as a result of operational conditions. However, turbine start and stop transients impart load ratios on the order of R=0.05, with stress ranges on the order of 500MPa to 800 MPa. A crack in existence and operating in the "safe zone" at R=0.8 may extend controllably, or uncontrollably during turbine startup. This can be seen graphically in Figure 16 below.

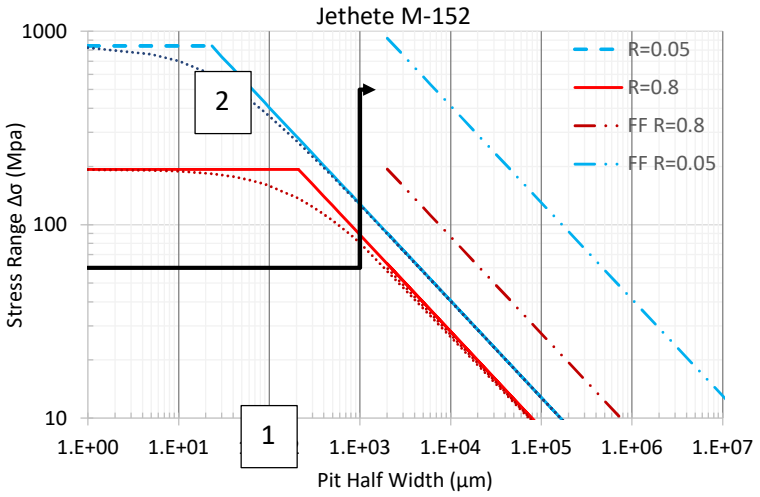

Figure 16: Kitagowa Diagram includes pit size-stress range combinations resulting in fast fracture.

Figure 16 provides the Kitagowa Diagrams to demarcate crack initiation and microstructurally small crack growth from geometrically large crack growth for load ratios of R=0.05 and R=0.8. Additionally, Figure 9 provides a line defining fast fracture (FF) for the Jethete material at both load ratios. The fast fracture predictions are estimated by use of Charpy Impact (CVN) to fracture toughness (KIC) relationships[9] [8] and is estimated conservatively to be K_{IC} = 50 MPa-$m^{1/2}$ from the Material Test Report. The operational region between the Kitagowa Line and the FF line represents controlled crack extension described by the Paris Relationship. Above and to the right of the FF line would predict catastrophic fast fracture. Figure 16 also provides a representative operational scheme, shown in black. The representative scheme depicts an L0 bucket operating at a stress range of 60 MPa and R=0.8. If, after a shutdown, a crack or pit on the order of 1000 µm in half width (0.039" half width or 0.079" in overall surface-intersecting size) is located in a region experiencing the known 60 MPa stress range during steady state operating conditions, the operator must decide an appropriate course of action relative to the crack found. The Kitagowa Diagram would indicate that, under normal operating conditions the crack would not extend extensively as a function of applied loading conditions (the state of being of the crack is located withing the "safe zone" of the Kitagowa Diagram- Location 1) and therefore monitoring of the crack *may* be an appropriate course of action. However, if the pit/crack experiences 500 MPa during start-up (R=0.05), the pit will experience loading conditions that will lead to crack extension in the Paris Regime (location 2). Depending upon the stress intensity resulting as a function of the loading and boundary conditions, crack extension during start-up may be considerable. As such, immediate action *may* be deemed necessary relative to the hypothetical crack. Specific progress on the Jethete L0 buckets included the discretization of the bucket/blade stress, from the leading edge inward, at the location of coupled elevated stress and highest water droplet erosion kinetics, shown in Figure 17.

[9] Hertzberg, R., W., *Deformation and Fracture Mechanics of Engineering Materials*. Fourth ed. 1996, Hoboken, NJ: John Wiley & Sons, Inc.

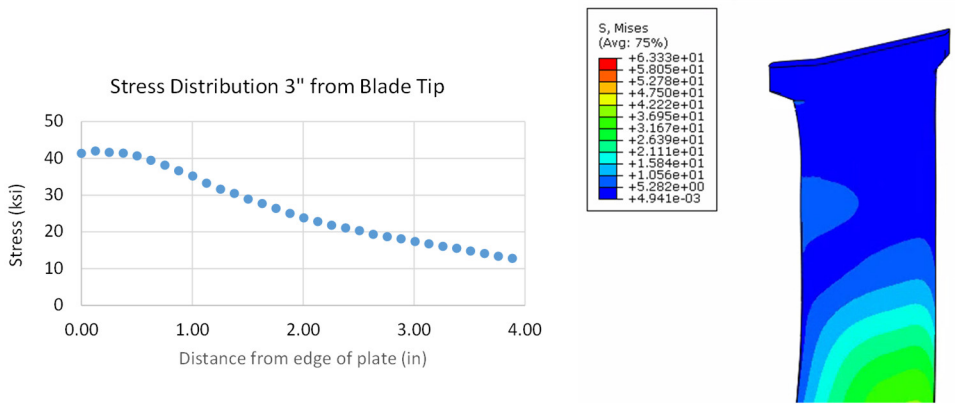

Figure 17: Stress distribution (from the blade leading edge inward) at the location of combined elevated stress and highest erosion kinetics.

The stress distribution shown in Figure 17 indicates that the stress decreases as one moves inward from the tip. This is beneficial as the data indicates that the driving force for crack extension decreases by approximately 50% as a crack advances to 2" in depth, as example. Crack geometries were then seeded within the blade finite element model to aid in stress concentration factor prediction. Cracks of varying length, having a tip radius of 5 µm, were modelled within the blade at the location of interest. The stress intensity factor resulting from each crack, as a function of the operational loading conditions, was then estimated. This data was then compared to the closed-form estimate of the stress intensity factor for a "Through Crack at the Edge of a Plate" from the AFGRO Damage Tolerant Handbook (AFGROW Hand Book of Damage Tolerant Design, downloaded 2021). Finite element and handbook comparisons of the stress intensity factors are provided in the figure 18 below.

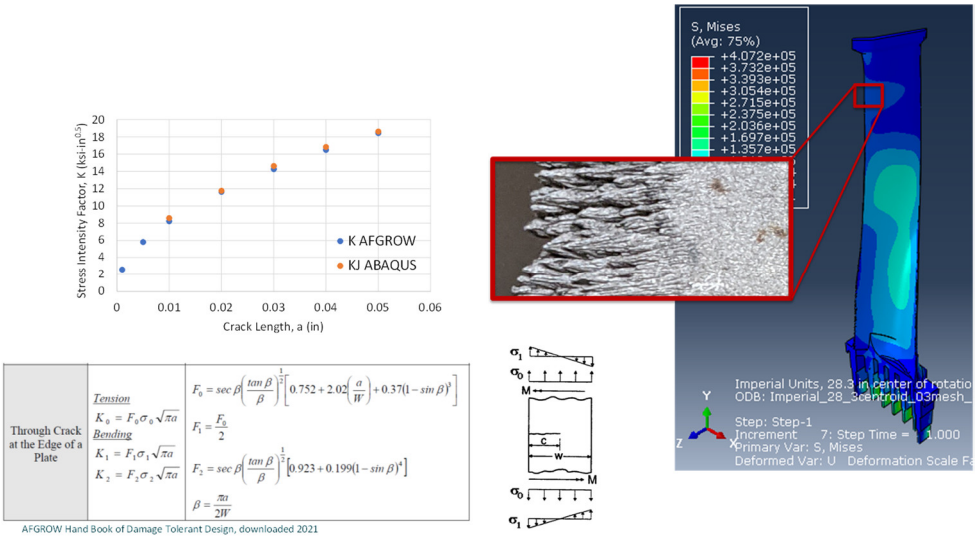

Figure 18: Comparison of stress intensity (K) estimates from closed-form solutions and FEM

The results displayed in Figure 18 indicates that the closed-form solution employed performs well at capturing the estimated stress intensity resulting from the existence of a crack. These results impact the project in two ways:

(1) the shape function used to create the Kitagowa Diagram must match that found in the AFGROW Handbook of Damage Tolerant Design, and not that found in the literature; and

(2) the closed-form solution may be used in numerical implementation of life modelling, thereby negating the need for computationally expensive finite element modelling.

Finally, the experimentally determined fatigue crack growth rate for Jethete at operational temperatures was used to determine the number of turbine starts remaining (prior to fast fracture) given a crack exists of known size. The data was collected for a series of initial crack sizes and is provided below in Figure 19.

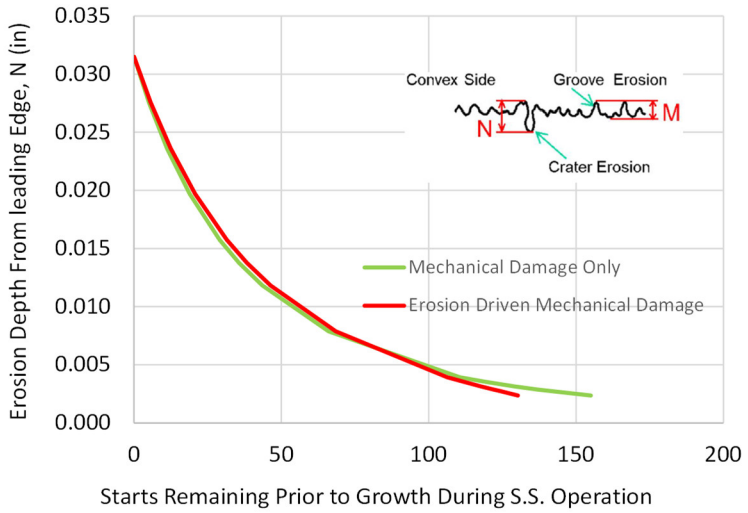

Figure 19: Correlated "Crater" Erosion Depth to turbine starts.

The data in Figure 19 may be used to determine M&O scheduling based upon inspection findings. As example, if a crater erosion crack is found to have a depth of 0.010", the data would indicate that the turbine bucket should be inspected within 25 turbine starts in order to ensure a factor of safety of 2 on failure.

3.6 Conclusions

Preliminary data collected to date on Jethete M-152 at operating temperatures and load ratios of interest indicate that the material exhibits very similar fatigue and damage response to those manifested by the dual certified AISI 403/410 12% Cr martensitic stainless steel extensively characterized by the Electric Power Institute and others[1],[2] [1, 2]. Specifically, the multi-year 403/410 stainless steel program included over 220 tests to characterize the materials FCG threshold and endurance limit in both virgin and pre-pitted conditions. Given the similarities between the 403/410 stainless steel test results and the Jethete studied here, it is evident that a Kitagowa Diagram approach to crack monitoring and blade inspection interval scheduling is a sound method. Furthermore, it appears that the extensive test data collected as part of the 403/410 stainless steel studies may be used here as foundational data for speculative extrapolation to include a general understanding of the Jethete material response to aerated environmental solution of 6 ppm Cl^- at 90°C[1] [1].

Tests conducted to date on the virgin Jethete M-152 turbine blade alloy include: (a) monotonic tensile testing at room temperature and operating temperature, (b) geometrically long crack growth at various load ratios at room temperature and operating temperatures, (c) fatigue crack growth threshold testing

and microstructurally small crack growth testing at room temperature at various load ratios, and (d) endurance limit (Stress-Life) testing at R=0.8 to cycles greater than 2.5 x 10^6.

4. RESULTS – P22 STEEL WYE BLOCK WELDS

4.1 Background

The Wye Block section is shown in Figure 20 as removed from a steam plant following decommissioning. The following section describes an important discussion on the rationale for the decision not to include the effects of the original cold spring design in the current modeling effort of a commercial Steam Main Steam Wye Block. Additionally, determination of geometry to use for CAD modeling when multiple sources are provided is addressed.

Figure 20. Photographs of the Wye Block section from the dismantled plant and during sample sectioning for the weld test sections.

4.2 Cold Spring Design Background

Per documentation provided by the industry, it is known that the main steam section of piping which contains the wye block of interest was installed with the utilization of a cold spring design. Such designs add complexity to initial and later analysis. The goals of such a design are described in the literature[10],[11],[12]. [1], [2], [3].

- Reduce the magnitude of loads placed on attached equipment and restraints by reducing the amount of thermal expansion realized at the connections
- Reduce hot stresses to mitigate creep damage.

---

[10] A. K. Dey, "A literature on 'Cold Springing (Cold Pull) In Piping Systems,'" *What is Piping*, 13-Jan-2020. [Online]. Available: https://whatispiping.com/cold-springing-cold-pull. [Accessed: 19-Jan-2021].

[11] "Cold Springing of Pipes " The Piping Engineering World," *The Piping Engineering World*, 09-Jan-2018. [Online]. Available: https://www.pipingengineer.org/cold-springing-of-pipes/. [Accessed: 19-Jan-2021].

[12] P. E. Meena Rezkallah, "3.6.1 Consideration of Cold Spring," *Little P.Eng. for Engineering Services*, 20-Dec-2020. [Online]. Available: https://www.littlepeng.com/single-post/2020/09/20/361-consideration-of-cold-spring. [Accessed: 19-Jan-2021].

These goals are realized through strategically cutting sections of pipe short or long prior to installation. These sections are then mechanically or thermally stretched or compressed prior to welding. When released, the cut-short sections will be in tension and cut-long sections will be in compression at room temperature. In the case of the main steam section of Gaston No.5, two cut-shorts are utilized. The industry documentation, *C-178675, Piping Stress Analysis Main Steam*, indicates the cut short amounts result in a 100% cold spring. This indicates that the cut short amount is equal to the expected thermal expansion when the pipe is in an operational condition of 1000°F. In theory, when the plant is off, the pipe will contain tensile residual stress as a result of the cut-shorts. When the plant is on, the tension from the cut shorts will be completely relieved by the resulting thermal expansion. Loading will still result from the operating internal pressure of 3500psi.

Use of cold spring design in practice is not universally accepted. Some designers may decide the additional work is not worth the gains. They point to the following issues with such a design[13] [4].

- Design codes such as ASME B31.1 require stress analysis be performed based on expected stress range which is unchanged by cold springs.
- Due to the complexity of pipe supports, installation errors and tolerances, it is exceptionally difficult to fully realize the goals of a cold spring design.
- Mechanical stretching of local sections the required amount is not always possible.
- High operating temperatures will result in the pipe relaxing to the theoretical cold spring position in a relatively short number of cycles anyway.

4.3 Wye block Decision Process

Inclusion of the original cold spring design adds complexity to the current modeling efforts. To determine if this effort will have significant impact on the resulting life predictions, the following questions must be answered.

1. What stresses are present in the on and off conditions if the cold spring is included?
2. What stresses are present in the on and off conditions if the cold spring is not included?
3. Does the difference in the included and not included cases result in a change in failure mechanism?
4. Does the difference in the included and not included cases result in a significant shortening of time to rupture in laboratory tests?
5. If the answers to 3 or 4 are yes, does the amount of time the cold spring acts as designed (prior to relaxation/annealing) have significant effect on total life predictions?

Finite Element Analysis of the pipe system with included cut-shorts is nontrivial. Because the design document, *C-178675*, indicates a 100% cut-short design, it is assumed that the stress resulting from a 930°F increase in temperature (operating temperature – room temperature) is equal to the stress resulting from the cut shorts. A model of the main steam pipe section was set up as follows based on design document *C-178675* and correspondence with industry representatives. See Figure 21

- The model is fully fixed at the turbine attachments.
- The stop valves are fixed from moving vertically (Y direction) and laterally (Z direction)
- The long vertical section is fixed from moving vertically (Y direction) 78.667ft above the wye block.

[13] G. H. May, "4.2.1 Cold Spring Design," in *Introduction to Piping Engineering*, SunCam.

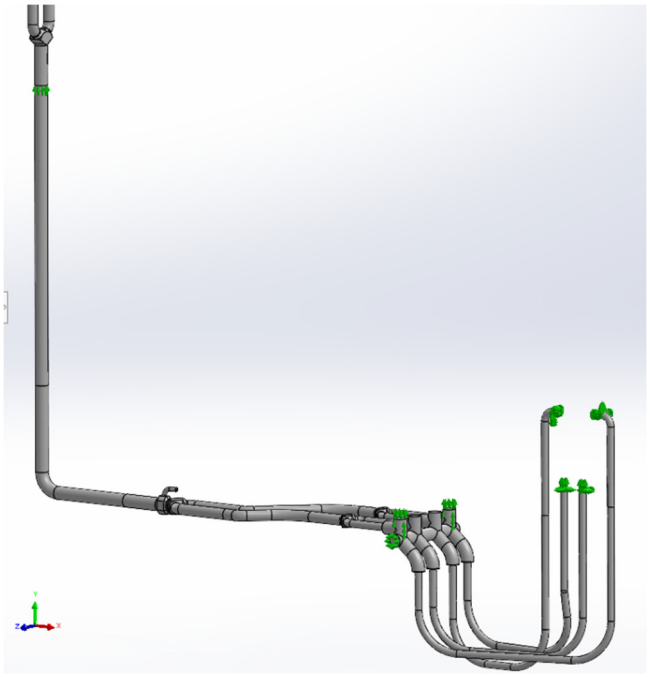

Figure 21: Model Boundary Conditions

Known cold to hot displacements from document *C-178675* were compared to simulated cold to hot displacements to show confidence in applied boundary conditions. The known and simulated displacements are a close match and have less than one inch difference in magnitude in the region of the wye block as shown in Figure 22.

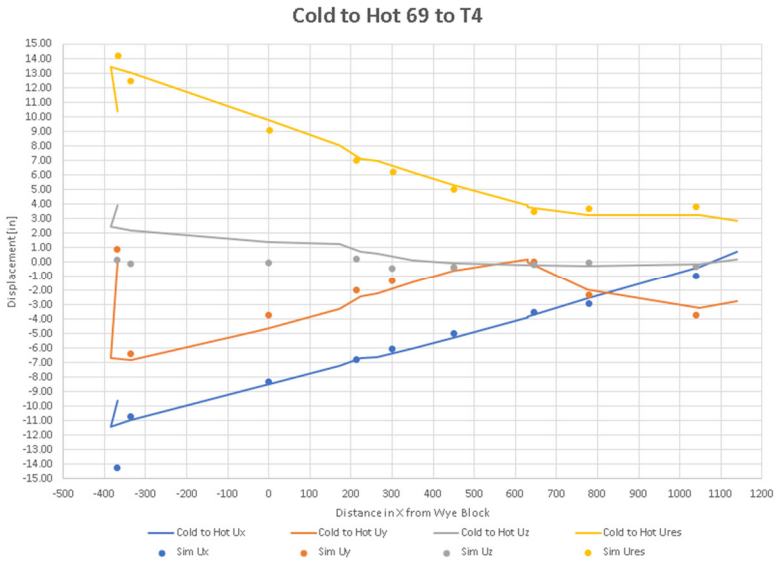

Figure 22: Known "Cold to Hot" displacements compared to simulated.

A reasonable mesh was determined previously to provide first order approximations of stress and displacements. The same mesh was used for the following scenarios:

1. Cold Spring Included, Plant off

2. Cold Spring Included, Plant on
3. Cold Spring not included, Plant off
4. Cold Spring not included, Plant on

A stress analysis of the installation revealed that the maximum stress was determined in the wye block body and pipe sections immediately adjacent. Findings are summarized in table 7.

Table 7: Maximum Stress at Wye Block for Various Conditions

Scenario	Maximum VM Stress psi [MPa]
1. Cold Spring Included, Plant off	785 [5.4]
2. Cold Spring Included, Plant on	14500 [100]
3. Cold Spring not included, Plant off	0 [0] *
4. Cold Spring not included, Plant on	14650 [101]

* 0 psi stress is the result of assuming no load on the system in the off state.

While the mesh used is only appropriate for first order solutions, it can be expected to provide reasonable magnitudes and allows for comparative results between situations. As such, table 7 approximates the answers to questions 1 and 2 in the previous section. Furthermore, it provides insight into the questions 3 and 4.

Figure 23 shows that in the 1000°F (575°C) temperature regime, multiple failure mechanisms may be in play depending on the actual stress. Additionally, at around 100MPa there is a transition between mechanisms. While these transitions are hard lines on the plot, in reality, a few MPa difference is unlikely to shift completely from one mechanism to another. Rather there will likely be some overlap and one would expect negligible difference in failure mechanism between scenarios 2 and 4. Similarly, the difference between scenarios 1 and 3 are small especially considering the assumption that the cold spring design is truly working 100%.

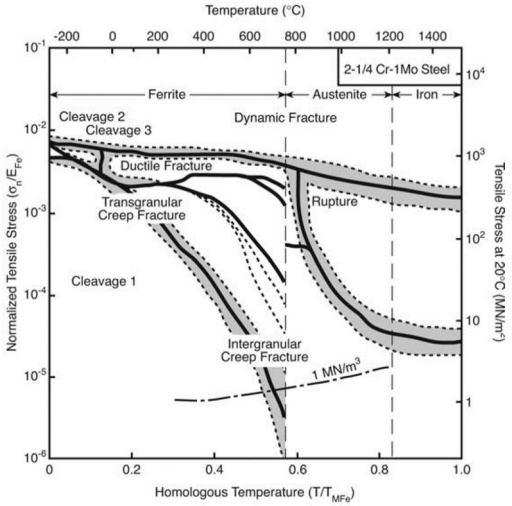

Figure 23: Failure Mechanism Map[14] [5]

[14] J. Parker, *The Grade 22 Low Alloy Steel Handbook 2-1/4Cr-1Mo, 10CrMo9, 622, STPA24 Technical Report*, vol. 1012840. Palo Alto , CA: Electric Power Research Institute, 2005.

Figure 24 shows that at operating temperatures, laboratory rupture behavior would not be expected to demonstrate significant differences as the result of the stress differences given in table 7.

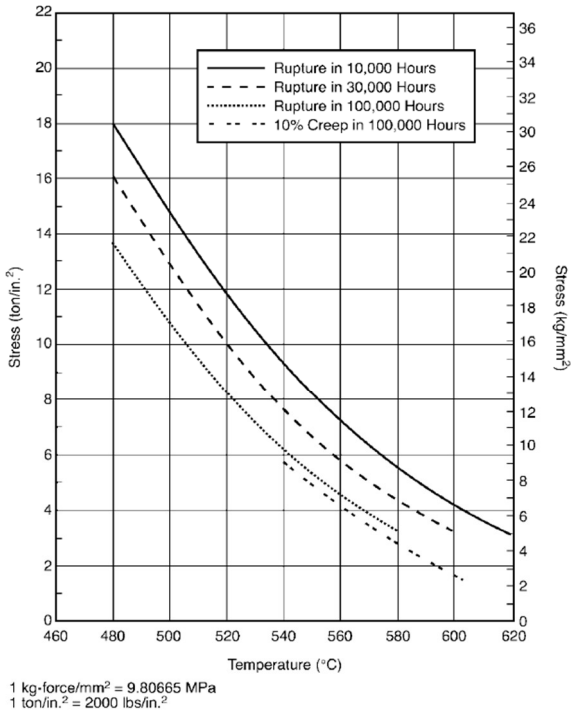

Figure 5-10
Estimates of the Long-Term Creep and Rupture Behavior of 2-1/4Cr-1Mo Steel [11]

Figure 24: Laboratory Creep Test Results

While the magnitudes of stress in this analysis may be inaccurate (on the order of 15%-20% maximum), it can be argued that the internal pressure within the pipe system is the primary generator of stress. When comparing the stresses resulting from internal pressures to those resulting from thermal expansion stresses, one notes that the latter are negligible at the wye block.

Additionally, it was documented that the material was installed in the annealed condition. Furthermore, post weld heat treat (1350°F) is performed at temperatures above the subcritical annealing temperature (1250°F). Coupled with this, stress relaxation resulting from operating temperatures near the subcritical annealing temperature is expected. In summary the effects of the original cold spring design will be excluded from the current modeling effort for the following reasons:

- The stresses at the wye block are only minimally affected by the cold springs and are unlikely to change the active damage mechanism(s).
- The effect of the cold springs will be reduced over time due to relaxation.
- Exclusion of the effect results in a slightly more conservative life estimate.
- The model will be more readily applicable to other plants that may not have originally included cold spring designs.

A final note should be made regarding geometry of the system. Two documents were provided that detailed the main steam geometry. One is the design document *C-178675* and the other is a .dxf CAD file. The lengths of each portion of the main steam pipe assembly differ such that the .dxf is generally shorter by 12-20 inches in each section. These differences are not completely resolved by assuming the cut short segments are accounted for in one and not the other. The overall assembly is large in comparison to these differences and it is not anticipated that the exact lengths are needed for the current modeling effort. Higher fidelity documentation exists for the wye block of interest and immediately adjacent areas. The modeling effort moving forward shall use the .dxf lengths for the base line of the CAD model geometry. Pipe cross sectional geometry between *C-178675* and the DXF are in agreement. Physical measurements of removed pipe sections of the wye block indicate that that there is a fair amount of wall thickness variation, the nominal dimensions reflect the actual components.

4.4 Calibration of Constitutive model for Post-Service P22 material

Work performed included the calibration of the preliminary constitutive model for the post-service P22 material (material removed from service). It has become clear that the deformation manifesting in the P22 (main steam) pipe material that was removed from service is vastly different than all data found in the literature. Specifically, the material removed from service has a reduced yield and ultimate tensile strength, as well as exhibiting considerably more ductility when compared to literature data. This indicates that the material is effectively annealed when operated in service as part of the main steam piping. As such, it is crucial that the in-service material's constitutive response be captured by use of constitutive modelling. Traditionally, constitutive models that capture damage evolution are calibrated by use of fully reversed strain controlled data (data collected at load ratios of R=-1). Unfortunately, the extreme ductility manifesting in the post-service material does not allow for fully reversed testing. Two exploratory, elevated temperature low cycle fatigue, tests were conducted to determine if the constitutive model created for this work could be calibrated by use of non-fully reversed testing (e.g. calibrated by use of effectively R=0 data). Specifically, a fully reversed test (R=-1) was conducted at a strain range of 0.2%. Additionally, another test having a (nearly) positive load ratio (R=-0.05) was conducted at a strain range of 0.25%. A preliminary constitutive model which incorporates nonlinear kinematic and isotropic hardening was calibrated by use of the R=-0.05 strain controlled data. The constitutive model was then used to predict the deformation response resulting in the fully reversed test. Example comparison hysteresis loops are provided below in figure 25 & 26.

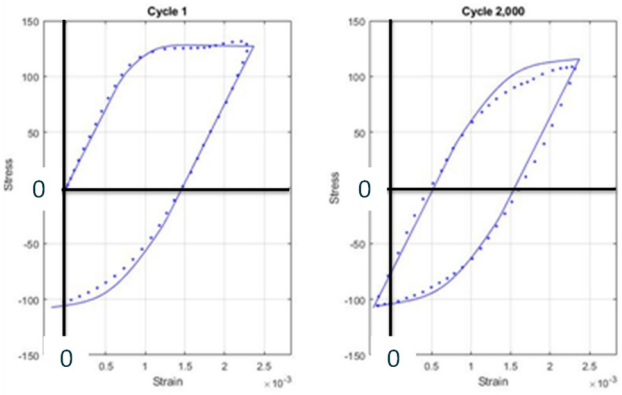

Figure 25: Constitutive model calibration to R=-0.05. Experimental data plotted as individual data points, model predictions plotted as a solid line. Initial cycle at left, fully stabilized cycle at right.

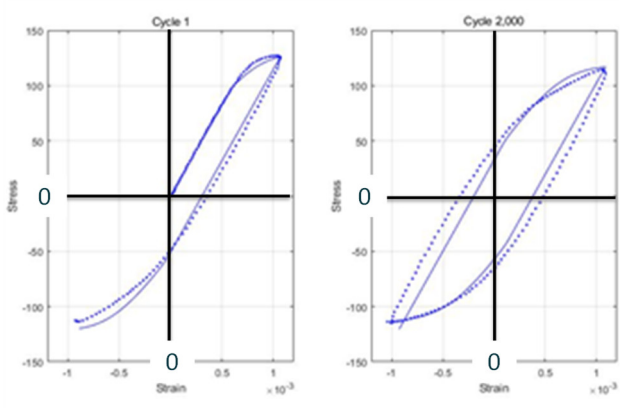

Figure 26: Constitutive model calibrated to R=-0.05 being used to predict deformation at R=-1. Experimental data plotted as individual data points, model predictions plotted as a solid line. Initial cycle at left, fully stabilized cycle at right.

The data provided in Figures 25 and 26 suggest that the elevated temperature constitutive model for the post-service P22 can be calibrated by use of non-fully reversed data. This discovery prompted all LCF testing for this program to be performed at a load ratio of R=0.05.

4.5 General Analysis of the Weld Region and material response

As part of the weld analysis, microhardness mapping of the cross-weld regions was conducted on the as-received P22 weld. Microhardness mapping data is provided in Figure 27.

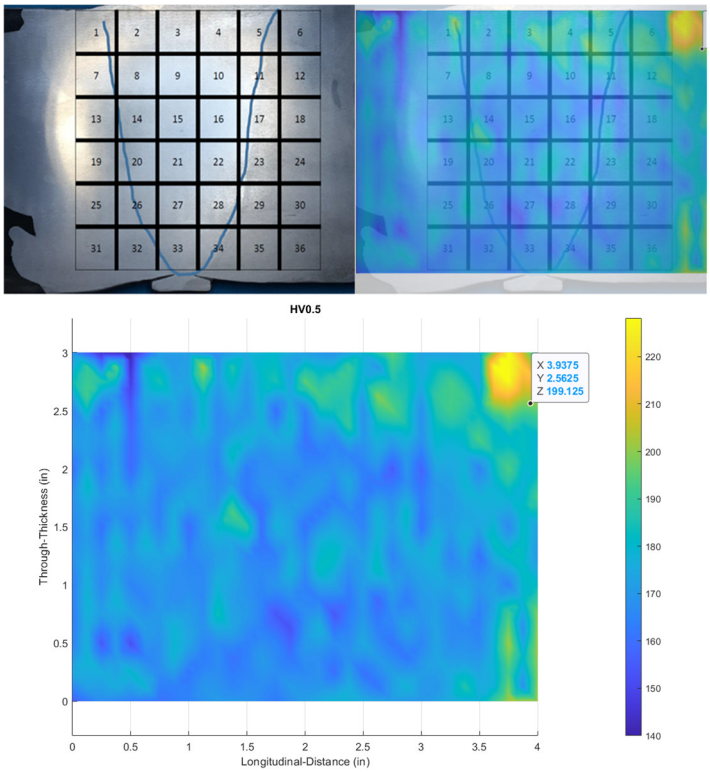

Figure 27: Cross-weld microhardness map of as-received weld. Images all have identical orientation and scale. Images of through-thickness pipe cross-section viewing colinear with the circumferential (or hoop) orientation. Grid shown has 0.5” x 0.5” spacing, units are HV0.5. P22 pipe at left, weld at center, T22 elbow forging at right.

The data provided in Figure 27 indicates that the customer-supplied P22 pipe base material (at left), the weld heat affected zones, and the weld fusion zone all manifest in relatively homogeneous hardness response. The homogeneity in hardness values is likely a result of 15 plus years of service conditions at temperatures in excess of 1000° F. While the bulk of the weld and it's associated fusion zones manifest in a microhardness on the order of 170 HV0.5, the weld cover pass(es) produce in slightly higher hardness values (on the order of 200 HV0.5). The forged elbow completing the weld assembly at right exhibits considerably harder material response at approximately 200 HV0.5 to 220 HV0.5.

The monotonic tensile properties of the P22 material tested at RT are documented in Table 8 and shown plotted in Figure 28 below.

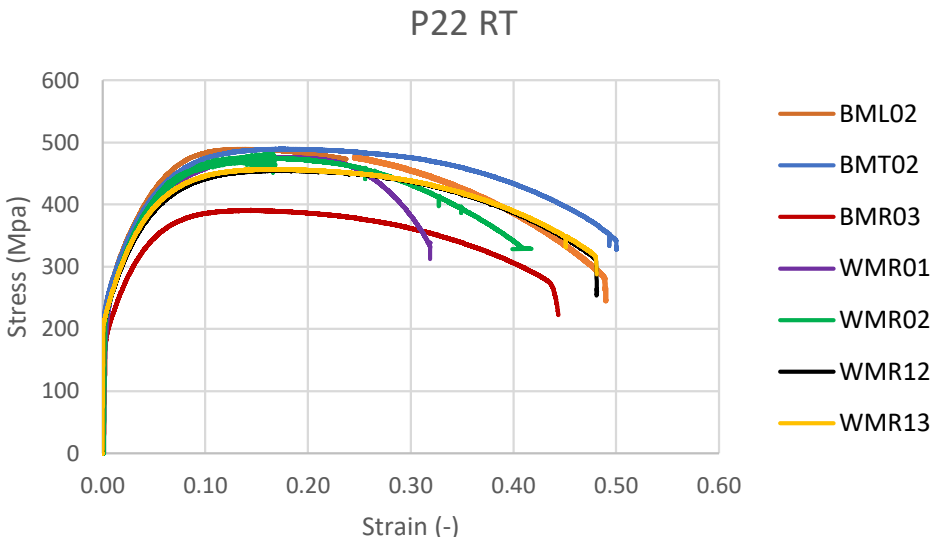

Figure 28: Monotonic tensile results of P22 material tested at room temperature. BM=base material, WM=weld material, L=longitudinal, T=transverse, R=radial

Table 8: Monotonic test data for P22 at room temperature

Specimen	Material	Location	Orientation	E (Gpa)	Sig_Y (Mpa)	UTS (Mpa)	E_f (-)
BML02	P22	Base Metal	Longitudinal	204.6	239.0	489.5	48.9
BMT02	P22	Base Metal	Transverse	199.2	241.0	489.8	50.0
BMR03	P22	Base Metal	Radial/Out	170.4	194.0	391.2	43.8
WMR01	P22	Weld HAZ	Radial/Out	200.0	188.0	476.1	32.0
WMR02	P22	Weld HAZ	Radial/Out	212.3	228.9	481.5	50.0
WMR12	P22	WELD	Radial/Out	212.0	222.7	455.8	48.1
WMR13	P22	WELD	Radial/Out	210.2	223.9	457.5	48.1

The strain controlled, low-cycle fatigue responses for the P22 material base material is shown in figure 29. The results are shown for BMT03, BMT05 and BMT06 respectively.

BMT03; εa=0.42%; Δε=0.84%; Nf~22,500

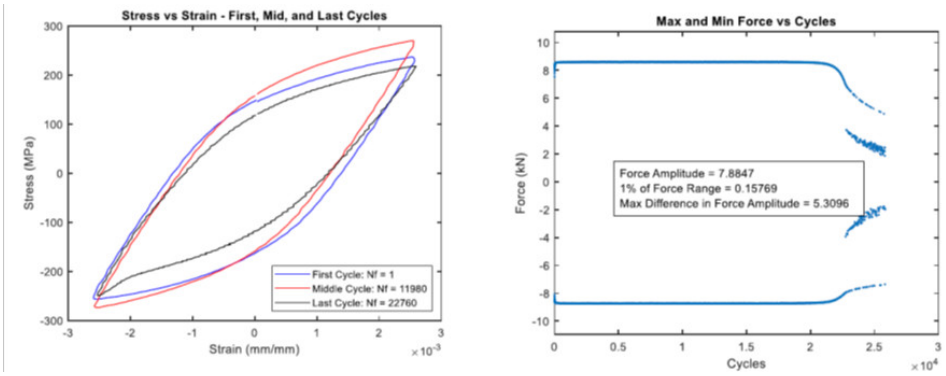

BMT05; εa=0.8%; Δε=1.6%; Nf~400/600

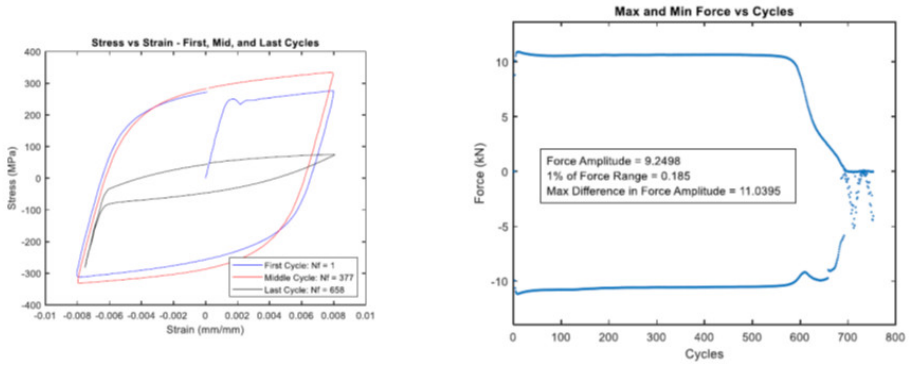

BMT06; εa=0.325%; Δε=0.65%; Nf~8800

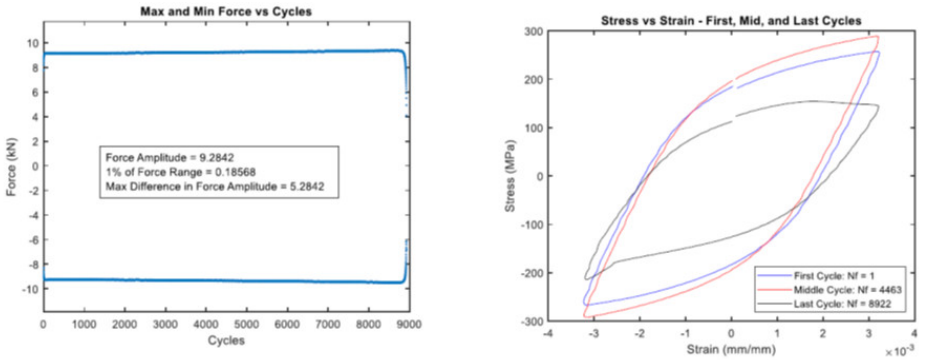

Figure 29. Strain controlled low-cycle fatigue data responses for the P22 base material under different test conditions showing the first middle and last cycle responses. Top ~23kcycles, middle ~650 cycles and bottom ~9kcycles